LIMNOLOGY
and
OCEANOGRAPHY: METHODS

Limnol. Oceanogr.: Methods 9, 2011, 232–244

A mesocosm tool to optically study phytoplankton dynamics

L. Peperzak[1], K. R. Timmermans[2], M. R. Wernand[2], S. Oosterhuis[2], and H. J. van der Woerd[1]*
[1]Institute for Environmental Studies–Instituut voor Milieuvraagstukken (IVM), Faculty of Earth and Life Sciences (FALW), VU University Amsterdam, De Boelelaan 1087, NL-1081 HV Amsterdam, The Netherlands
[2]Royal Netherlands Institute for Sea Research/NIOZ, Den Burg, The Netherlands

Abstract

The accuracy of remote sensing algorithms for phytoplankton biomass and physiology is difficult to test under natural conditions due to rapid changes in physical and biological forcings and the practical inability to manipulate nutrient conditions and phytoplankton composition in the sea. Therefore, an indoor mesocosm was designed to examine the optical properties of phytoplankton under controlled and manipulated conditions of irradiance, temperature, turbulence, and nutrient availability. Equipped with hyperspectral radiometers and bottom irradiance meters, it is shown that under semi-natural environmental conditions biogeochemically relevant species as *Emiliania huxleyi* and *Phaeocystis globosa* can be grown with good precision (± 20%) between duplicate mesocosms and between duplicate sensors (<5% deviation). The accuracy of chlorophyll estimates by absorption, using an Integrating Cavity Absorption Meter, and fluorescence using water-leaving radiance was 74% to 80%, respectively, as it was negatively influenced by changes in phytoplankton physiology. Biomass detection was limitedto 1 to 2 µg chlorophyll/L with an apparent linearity to 50 µg chlorophyll/L. Estimates of the quantum efficiency of fluorescence ($\varphi \approx 0.01$) were comparable to real-world estimates derived from satellite observations. It is concluded that the mesocosms adequately simulate natural conditions with sufficient accuracy and precision and that they offer an important tool in validating assumptions and hypotheses underlying remote sensing algorithms and models.

Optical instruments on board satellites have shown to be indispensable in the study of phytoplankton dynamics and related biogeochemical cycles on a global scale (Behrenfeld et al. 2009; Kirk 1994). Satellite observations daily cover the whole surface of the oceans, but they still do not allow the accurate retrieval of the large amount of variables, such as nutrient concentrations and physiological rates, that can be measured in situ. On the other hand, drawbacks of in situ phytoplankton investigations, such as the measurements of primary and secondary production, are the small number of water samples that can be examined and the relatively small areas of the sea that can be covered daily. Mesocosms are experimental tools mimicking natural water bodies that allow manipulation of, for instance, nutrient concentrations and irradiance enabling high-frequency sampling. The aim of this paper is to describe and test an indoor mesocosm facility for the study of phytoplankton dynamics under controlled conditions by using both in situ techniques for algal biomass and physiology estimations, as well as water-leaving radiance measurements. Such a facility would be essential to study the quantitative relations between fluorescence, biomass, and growing conditions to interpret variability in remotely sensed algal fluorescence (Huot et al. 2005), and in examining the effect of nutrient perturbations on phytoplankton dynamics and associated optical properties.

A widely used proxy for phytoplankton biomass in both in situ and remote-sensing studies is the chlorophyll *a* concentration. Chlorophyll *a* (Chl *a*) is estimated from remotely sensed water-leaving radiance in a number of ways (Huot et al. 2005; Kirk 1994; Van Der Woerd and Pasterkamp 2008). First, by measuring the water-leaving radiance absorption spectrum that is influenced by the absorption characteristics of the phytoplankton species, phytoplankton biomass, non-phytoplankton seston, and gilvin (yellow substances) (Kirk 1994). Technically, the amount of absorbed radiation by phytoplankton is not only

*Corresponding author: E-mail: Louis.Peperzak@nioz.nl
Phone: +31-222-369495; Fax: +31-222-319674

Acknowledgments

We gratefully acknowledge the help of the following NIOZ personnel. The mesocosm was constructed by H. de Porto, J. Schilling, L. Boom, R. Daalder, D. Heerschap, R. Lakeman, R. Bakker, and E. Keijzer. POC and PON were analyzed by S. Crayford. Nutrients were analyzed by K. Bakker, E. van Weerlee, and J. van Ooijen. H.J.v.d.W was supported by the BSIK Climate Changes Spatial Planning A6 project. Financial support for this research was obtained from NOW User Support Programme Space Research project EO-078: 'Improved quantification of Southern Ocean diatoms as indicators for Carbon fixation', granted to H.J.v.d.W.

DOI 10.4319/lom.2011.9.232

dependent on the Chl *a* concentration, but also on other radiation-absorbing phytoplankton pigments (Huot et al. 2005). In water samples, these phytoplankton pigments are accurately measured by high-performance liquid chromatography (HPLC) (Gieskes and Kraay 1986; Zapata et al. 2004). However, changes in phytoplankton composition and phytoplankton adaptations to changes in irradiance and in nutrient regimes hinder the correct estimation of Chl *a* concentrations from water-leaving radiance spectra (Sathyendranath et al. 2004).

A second method to estimate Chl *a* from water-leaving radiance is to measure the intensity of the sun-induced chlorophyll fluorescence near 683 nm, calculated for instance by using the fluorescence line height (FLH) method (Carder et al. 2003). However, under conditions of nutrient-limiting growth, the intensity of the emitted fluorescence increases relative to the energy absorbed by the chlorophyll-containing photosystem II (Falkowski et al. 1992). On the other hand, if under such nutrient-limiting conditions phytoplankton absorption remains unchanged, the increase in fluorescence intensity relative to radiance absorption can be used as a proxy for the physiological status of the phytoplankton. In water-leaving radiance spectra, this physiological indicator, the chlorophyll fluorescence efficiency (φ) is the ratio of the number of fluoresced photons to the number of photons absorbed by the phytoplankton (Abbott and Letelier 1999).

The accuracy of remotely sensed proxies such as Chl *a* concentration is assessed by correlating the outcome of the respective algorithms with less frequently available in situ data (Carder et al. 2003; O'Reilly et al. 1998; Parkinson and Greenstone 2000). For the physiologically variable chlorophyll fluorescence, hence φ, the correlation analysis is even more difficult due to a lack of in situ data (Huot et al. 2005). The applicability of φ as an iron stress indicator, for instance, had to be deduced indirectly from a global comparison of the φ distribution with that of the modeled aeolian soluble iron deposition (Behrenfeld et al. 2009).

Experimental testing of remote sensing of chlorophyll concentration and φ appears even scarcer. Manipulation of the aquatic environment such as by nutrient additions is difficult to perform. Not only do large areas need to be treated to be visible from space, there is also an inherent experimental and observational variability due to intermittent changes in water currents and in atmospheric conditions. Nevertheless, remote sensing by satellites has been used to gauge the effect of large-scale iron enrichments on phytoplankton growth in the Southern Ocean (Abraham et al. 2000). Such experiments, however, cannot be performed on a regular basis. Therefore, an experimental set-up was devised that would allow manipulated phytoplankton growth under controlled, but semi-natural conditions. The water volume should be large enough to perform both remote sensing observations and in situ (water-) sampling. Also known as mesocosms, such experimental set-ups have been successfully used in studying phytoplankton behavior under several kinds of physiological stress, such as induced by ultraviolet radiation or by nutrient limitation (Belzile et al. 1998; Escaravage et al. 1995). Combined with optical measurements, previous mesocosm experiments with phytoplankton have been conducted to examine the effect of growth and aggregation on bulk and individual optical variables (Costello et al. 1995), but without measuring water-leaving radiance. Schalles et al. (2001) investigated the sensitivity of chlorophyll algorithms by measuring the effect of clays on water-leaving radiance in phytoplankton containing mesocosms; Cui et al.(2003) measured reflectance spectra of a phytoplankton 'red tide' incubated in a mesocosm; and Hunter et al. (2008) measured reflectance spectra of phytoplankton cultures. In none of the studies above, however, the phytoplankton was experimentally manipulated.

In this article, it will be tested if phytoplankton dynamics in a mesocosm can be induced under semi-natural conditions of irradiance, temperature, turbulence, and nutrient availability. In addition, optical properties such as absorption and fluorescence should reflect the phytoplankton dynamics measured in situ in a reproducible manner.

Material and procedures

Mesocosm set-up

The mesocosm tank, height 0.75 m, diameter 0.5 m, and water volume 0.14 m^3 was made of black high density polyethylene (Wijtmans Plastics) and mounted in a metal frame made of 30 mm square aluminum painted black (Fig. 1). To avoid light reflection from the walls the interior of the tank was sand-blasted. The contents was mixed by pumping water at a turn-over rate of 1 $h^{-1}$from 0.05 m below the water surface (–0.05 m) to 0.10 m above the bottom (–0.60 m) using a Liquiport™ model NF300KT.18S membrane pump (KNF Neuberger). Samples were collected via a three-way valve in the tubing between pump and mesocosm inlet (bottom) or outlet (surface) (Fig. 1). The tubing was 15 mm diameter silicon-rubber of 2 × 3 m length between pump and mesocosm to damp vibrations of the pump. The water was pumped into the mesocosm at the bottom so that a current over the bottom irradiance sensor prevented particles from settling on, and influencing, sensor readings. Directly after sampling, the total water volume was restored by adding filtered seawater (typically 1 L or < 1% of the total volume) up to the overflow, that was situated 0.05 m below the rim of the mesocosm (Fig. 1).

Because hyperspectral radiance and irradiance measurements had to be performed under circumstances simulating natural conditions, ordinary light bulbs and fluorescent tubes with highly red-skewed or peaked spectra could not be used as light source. Instead, 50 W Solux™MR16 halogen 4700K "daylight" lamps with a 24° beam spread were used in a 5 × 5 matrix in a black-painted box that was mounted in a frame at 0.70 m above the water surface (Fig. 1). The lamps were connected to 230 to 12 V transformers. The spectrum of the 4700K Solux lamp is comparable with the solar spectrum

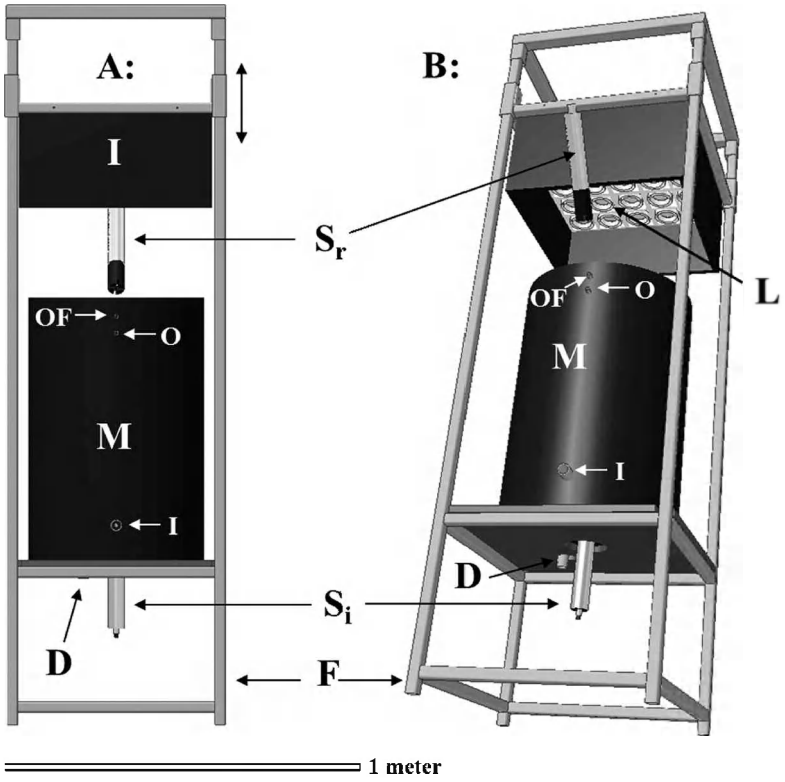

Fig. 1. Schematic representation of the mesocosm system. A. side view, B. view from below. The mesocom vessel (M, height 0.75 m, diameter 0.50 m) is placed inside a metal frame (F) that also holds the illumination box (I). The illumination box contains 25 Solux™ lamps (L) and is height-adjustable (↕). Two hyperspectral sensors were installed: one for bottom irradiance (S_i) and one for water-leaving radiance (S_r). Water was pumped round through an outlet at –0.10 m (O) from the rim and an inlet (I) at +0.10 m from the bottom. An overflow (OF) at –0.05 m from the rim was used to keep the water level constant. The mesocosm is emptied with a drain (D) in the bottom. For clarity, the construction holding the radiance sensor (S_r), electrical wiring, tubing, valves, and pump are not shown.

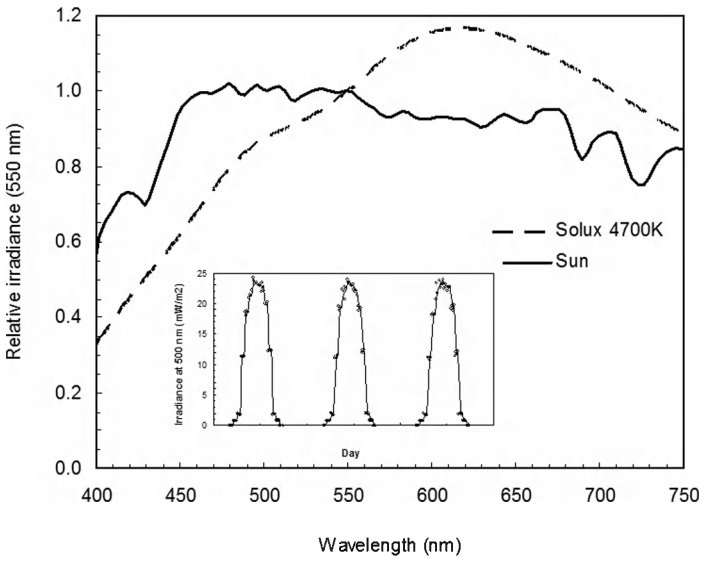

Fig. 2. Spectra of the sun and a Solux 4700K halogen lamp used to illuminate the mesocosm. The spectra were measured with a Trios RAMSES-ACC-VIS hyperspectral irradiance sensor and transformed in relative units by division with the intensities at 550 nm. The inset shows an example of the semi-sinusoidal illumination regime in a 12:12 light:dark cycle.

(Fig. 2). Water surface irradiance was adjustable by changing the height of the lamps or by using 35 W instead of 50 W Solux lamps. Because diel variations in the biological and optical properties of photosynthetic phytoplankton take place in nature (Claustre et al. 2002; Vaulot and Marie 1999), and square wave (on-off) illumination, in theory, may affect the rate of diel optical variations (Esposito 2006), variable light:dark cycles with a semi-sinusoidal illumination were made possible by six electronic timers controlling a maximum of 24 Solux lamps in groups of four and one timer controlling the central Solux lamp (Fig. 2).

Temperature

All experiments were run in a temperature-controlled room at 15°C. The water temperature was measured every 15 min with a LogTag™ St100T-15 stainless steel thermometer and stored in a LogTag Trex-8 data logger (LogTag Ltd.). Temperature was measured in the first 0.05 m of the water surface. To examine a temperature difference between surface and bottom the thermometer was lowered to 0.05 m above the bottom.

Salinity, pH, and nutrients

Salinity was measured with an Endeco™ type 102 refractometer or a GMH3430™ conductivity meter (Greisinger electronic GmbH). pH was measured with a Metrohm™ 827 pH

lab (Metrohm). Samples for the inorganic nutrients nitrate, nitrite and ammonium (Dissolved Inorganic Nitrogen, DIN) and phosphate (Soluble Reactive Phosphate, SRP) were filtered through 0.2 µm Acrodisk filters, frozen, and stored at –80°C. Samples for dissolved inorganic silicate (Si) were also filtered through 0.2 µm Acrodisk filters, but stored at 4°C. Nutrient analyses were performed according to state of the art NIOZ protocols based on Grashoff et al. (1983), Helder and De Vries (1979), Murphy and Riley (1962), and Strickland and Parsons (1968).

Optical

Before or after the experiments, surface irradiance (E_0) was measured every 15 min for at least 24 h from 320-950 nm in 190 channels (W m^{-2} nm^{-1}) with a TriOS™ RAMSES-ACC-VIS hyperspectral cosine irradiance sensor (TriOS GmbH) that was placed in the center of the mesocosm at the position of the water surface. During experiments the irradiance at the bottom (E_b) of the mesocosm (Fig. 1) was measured every 15 min with a similar TriOS hyperspectral cosine irradiance sensor.

Water leaving radiance (L_w) was measured every 15 min with a TriOS RAMSES-ACC-VIS hyperspectral radiance sensor (radiometer, 320-950 nm in 190 channels, W m^{-2} nm^{-1} sr^{-1}) at an angle of 50° nadir at 0.08 m above the water surface (Fig. 1). All instruments were connected to a personal computer through a TriOS IPS104-4-plus interface with a Sitecom™ CN-104 USB-to-serial-port adapter cable (Sitecom). Data acquisition, calibration, and storage was controlled by TriOS™ MSDA_XE software running under Windows XP. Because the Solux lamps were not directly stable after switch-on, radiance and irradiance measurements were delayed 5 min.

Absorption

An integrating cavity absorption meter or ICAM (a-sphere spectrophotometer, HOBI Labs) was used as an independent method to measure sample absorption. This type of instrument is very accurate, also at low concentrations, without interference by particle scattering (Röttgers et al. 2007). The ICAM was connected to a Delta electronica 30V power supply (Delta electronics) and a Keyspan USA-19HS USB-to-serial-port adapter cable (Tripp-Lite) via the HOBI Labs Power/Data interface cable. The ICAM was filled with 550 mL sample at a rate of 500 mL/min with a Masterflex Easy-Load™ II pump with KH-06419-18 (ø = 7.9 mm) Tygon tubing (Cole-Palmer). Tests using flow cytometry (see below) showed that filling the ICAM using this treatment did not affect cell counts, forward scatter, side scatter or the red autofluorescence of small phytoplankton cells. Instrument variability was checked regularly by measuring Milli-Q water and 0.2 µm filtered seawater as used in the experiments. Each absorption spectrum (360 to 750 nm) measurement was replicated six times in immediate succession and averaged. All measurements were made at in situ temperatures. The ICAM data were directly checked for abnormalities and converted to absorption (m^{-1}) using Igor Pro™ 6.12 (Wavemetrics).

Phytoplankton cultures

Stock cultures of the prymnesiophytes *Phaeocystis globosa* Scherffel (clone NIOZ Pg6 (I), flagellates) and *Emiliania huxleyi* (Lohmann) W.W. Hay & H.P. Mohler (clone NIOZ Eh12) were maintained in membrane (0.2 µm) filtered and autoclaved North Sea water with nutrient additions that were slightly adapted from PEP-Si culture medium, based on winter nitrate concentrations (100 µM) in the coastal North Sea (Peperzak et al. 2000a). After addition of 1 mL stocks of macronutrient, trace metals and vitamins to 1 L seawater the minimum concentrations were 100 µM NO_3^-, 6.3 µM PO_4^{3-}; 1 µM Fe, 100 nM Zn, 100 nM Co, 100 nM Mn, 10 nM Se, 10 nM Cu, 1 nM Mo and an equivalent concentration of EDTA; 100 nM B1 and 1 nM biotin.

Biological measurements

Cell concentrations were measured with a Coulter Epics™ XL-MCL flow cytometer (Beckmann Coulter). Counts were triggered on red autofluorescence (FL4), measured at > 610 nm. Scatter of the 488 nm Argon laser beam was measured as forward scatter (FS) and side scatter (SS), giving information on cell size and morphology respectively (Peperzak et al. 2000b).

A Pulse Amplitude Modulation (PAM) WATER-ED™ fluorimeter (Walz) was used to assess the quantum efficiency of photosystem II (Fv/Fm) of the phytoplankton and in vivo chlorophyll-fluorescence (F_0) (Schreiber et al. 1986) after at least 15 min storage in the dark near in situ temperatures.

Phytoplankton pigments, POC, and PON

Samples for pigment analysis were filtered on 25 mm Whatman™ GF/C filters at < 0.2 kPa and stored at –80°C. Pigment extraction took place in 4 mL 100:20 (v/v) methanol:water using glass pearls in a CO_2-cooled Braun™ (Melsungen, Germany) homogenizer. Extracts were centrifuged and filtered through 13 mm diameter 0.45 µm PTFE syringe filters (Grace Davison Discovery Sciences) to remove cell and filter debris. The final homogenates containing the extracted pigments were placed in a Dionex™ autosampler thermostated at 4°C. The analyses were made using a Dionex™ HPLC system equipped with a C_8 separation column (Luna 3 µ C_8(2) 100A 100 × 4.6 mm) thermostated at 25°C. Pigments were detected at 437 nm with a Dionex™ photo diode array detector. The solvents used were (a) methanol:acetonitrile:aqueous pyridine (50:25:25 v/v/v) and (b) methanol:acetonitrile:acetone (20:60:20 v/v/v) (Zapata et al. 2000). Standards were obtained from DHI™ (Denmark).

Experimental

Seawater originating from the Atlantic Ocean (Canary Basin) was filtered through a 0.2 µm filter (MidiCap™) and diluted with demineralized water to salinities below 35. To impose nitrogen-limitation in stationary growth phase the initial NO_3^- concentrations were reduced from 100 µM to 30 µM.

The prymnesiophyte species were used in two separate experiments. In a single mesocosm, *E. huxleyi* was grown to test water column homogeneity by taking daily surface and bottom samples at midday from both the in- and outlet (Fig. 1). In addi-

tion, data from two radiometers placed at a relative azimuth angle of 90°, collected on 1 d at maximum biomass, were used to test radiometer precision. The radiance of both sensors was summed between 400 and 700 nm. *E. huxleyi* growth conditions were: salinity 31, 15°C and a maximum of 30 W m^{-2} surface irradiance (PAR) in a 12:12 light:dark cycle (Fig. 2).

In two duplicate mesocosms, *P. globosa* was grown at salinity 34, 15°C and a maximum of 41 (mesocosm 1) and 45 W m^{-2} (mesocosm 2) surface irradiance (PAR) in a 16:8 light:dark cycle. On day 8 when *P. globosa* in both mesocosms had stopped growing due to nitrogen limitation, mesocosm 1 received a 30 µM NO_3^- spike to resume growth. Further details on the *E. huxleyi* and *P. globosa* experiments will be presented elsewhere (Peperzak et al. unpub. data).

Statistics

Linear regression analysis (SYSTAT™ version 12 or Excel™ 2003) was used to test the null hypothesis that two variables, measured at the surface or bottom, with two independent radiometers, or measured in duplicate mesocosms, were not statistically different. The standard error of the slope of the regression line was multiplied by the value of t (df = n-1, α = 0.95) from a t-distribution to obtain 95% confidence intervals. If this interval included the value of 1.0, then the slope was considered not significantly different from 1. If the linear regression intercept was not significantly different from 0, it was assumed that there were no systematic differences between the two sets of variables.

Models of absorption and fluorescence

A major difference between real-world radiance measurements and those in the experiments is related to the limited mesocosm depth and its black walls and bottom. Therefore, an optical model of the mesocosm was constructed, based on the data of the *P. globosa* experiment including the ICAM absorption data. Such an optical model is essential to have a proper interpretation of the light measurements and full understanding of the light absorption and emission in the mesocosm. To determine the fluorescence quantum efficiency of the phytoplankton, one has to derive, from measurements, the number of photons absorbed (over all wavelengths) and the number of photons emitted in the fluorescence band. The bottom irradiance measurement is not only influenced by the phytoplankton pigments, losses also occur by water absorption, CDOM absorption, geometric losses (the lamps have not a perfect parallel beam) and scattering by small particles. The model should demonstrate that from the irradiance spectra at the start and during the experiment that it is possible to derive the energy absorbed by the phytoplankton. Similar arguments are valid for the fluorescence signal: The photons are emitted in all directions, over a large range of wavelengths with strong and variable absorption by water. Therefore, the signal that is measured by the radiance spectrometer above water is reduced and slightly deformed. A simple model is presented that should reproduce the above water fluorescence spectra.

Assessment

Abiotic variables

The maximum PAR (Photosynthetic Active Radiation, 400-700 nm) achieved at the mesocosm water surface was 200 µmol photons m^{-2} s^{-1} or 45 W m^{-2}, which is 20% of the summer maximum at 53°N (North Sea). Using values of the bottom irradiance in filtered seawater (26 W m^{-2}), the apparent attenuation coefficient in the mesocosms was 0.75 m^{-1}, and the mean water column irradiance was calculated to be 34 W m^{-2}. This mean irradiance in the mesocosms compared well with an average of 32 W m^{-2} for the North Sea [225 W m^{-2}, Kd = 0.22, z = 32 m (Peperzak 1993)]. Diurnal variations in surface water temperature that were caused by the semi-sinusoidal illumination were relatively small (± 0.4°C). In May 2008, for instance, during sunny weather, the diurnal surface temperature difference in the North Sea was ± 0.6°C (L. Peperzak unpubl. data). Evaporation caused an increase in salinity (0.07 d^{-1}) that was negligible (<5%) in the course of a typical 2 week experiment at 15°C. It is concluded that the mean water column mesocosm irradiance adequately simulated natural conditions and that lamp-induced temperature and salinity changes were negligible.

Homogeneity

Microscopic examination of *E. huxleyi* showed that cells were not damaged by the mesocosm pump at a turnover rate of 1 h^{-1}. At this rate, the differences between surface and bottom samples were not significant (Fig. 3a), meaning that the water column was well mixed. Exceptions appear to be DIN (intercept –2.9 ± 2.0) and Fv/Fm (slope 0.95 ± 0.02 and intercept 0.03 ± 0.02), but these differences were very small. The turnover rate of 1 h^{-1} applied in the *Phaeocystis* experiment also led to negligible differences (<5%) in cell biomass between surface and bottom at high (>40 µg chlorophyll/L) biomass. Therefore, the membrane pump and the pump speed employed (140 L/h) were considered adequate to maintain cell integrity and water column homogeneity.

Radiometer precision

Two simultaneous radiometer measurements of water-leaving radiance from a mesocosm containing *E. huxleyi* revealed a very good precision (slope 1.04 ± 0.01) and correlation (r^2 = 1.00) (Fig. 4). This meant that one radiometer per mesocosm would suffice in future experiments.

Mesocosm reproducibility

After 4 d of exponential growth, *P. globosa* reached a maximum of 65 µg chlorophyll/L in both mesocosms (Fig. 5a). Examples of reflectance spectra showed that the full range of chlorophyll concentrations was detectable by water-leaving radiance measurements (Fig. 5b). The lower surface irradiance in mesocosm 1 resulted in a delayed peak in chlorophyll-concentration (day 5). A second peak was reached on day 9 after the nitrogen-spike on day 8 (Fig. 5a). Data from this duplicate experiment, from day 1 to 8, were very comparable with slopes between variables at ± 20% (Fig. 3b). Only one variable

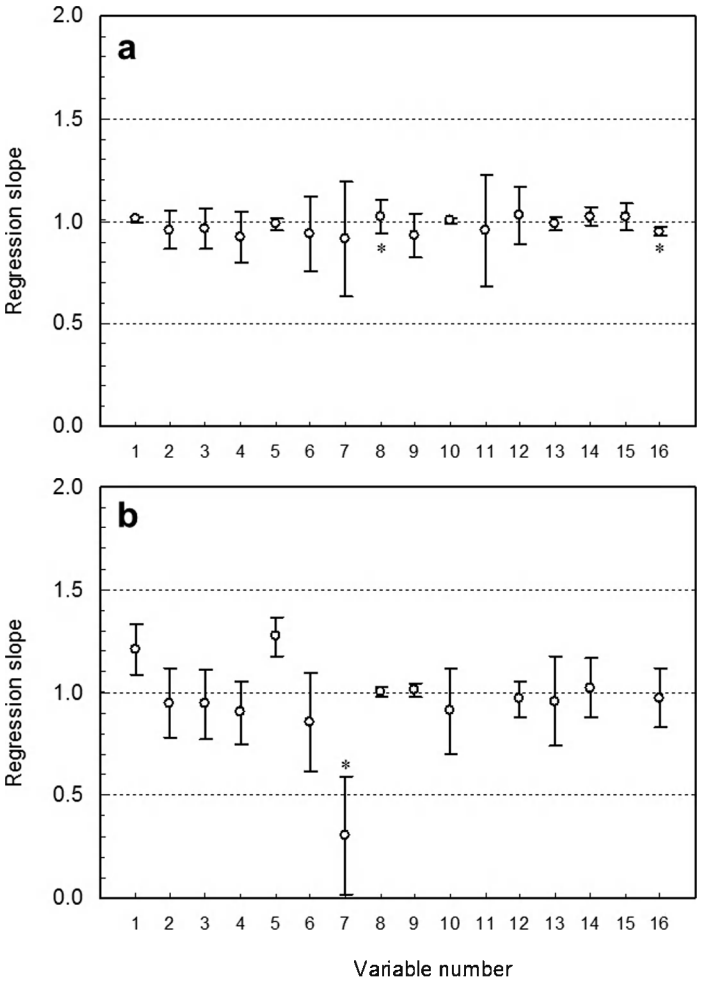

Fig. 3. Comparison of bottom vs. surface samples (a) and duplicate mesocosms (b) as slopes of the linear regression between water variables. Bars are 95% confidence intervals: if these cross the horizontal line (1.0), than the slope of the regression line (variable2 = slope × variable1 + intercept) is not significantly different from 1. The variables measured were 1. cells/L; 2. µg chlorophyll *a*/L; 3. µg chlorophylla+c/L; 4. µg carotenoids/L; 5. F0; 6. salinity; 7. pH; 8. DIN µM; 9. SRP µM; 10. NH4+ µM; 11. CDOM; 12. Forward Scatter; 13. Side Scatter; 14. Red autofluorescence; 15. coccoliths/L; 16. Fv/Fm. a. *E. huxleyi*: the * at variables 8 and 16 (DIN and Fv/Fm) indicates that the regression line intercept was significantly higher than 0. All other regression lines had intercepts that were not significantly different from 0. b. *P. globosa*: duplicate mesocosms during 8 d of exponential growth. Variables 11 and 15 were not measured. See text for comments on variable 7 (pH).

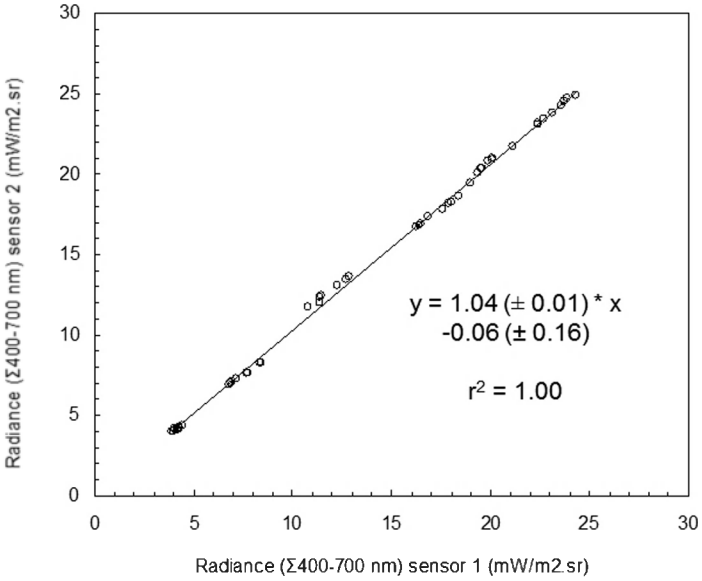

Fig. 4. Comparison of two duplicate radiometers measuring water-leaving radiance in one mesocosm containing *E. huxleyi*. Radiance was summed from 400 to 700 nm. Data were collected every 15 min during a 12-h light period.

had a low slope (pH, variable 7) and an intercept significantly different from zero. In this case, linear regression was difficult to perform because of the small differences in pH between mesocosm 1 (pH = 8.17 ± 0.04) and mesocosm 2 (pH = 8.24 ± 0.02). Mesocosm 2 contained significantly more cells (variable 1), a higher F_0 (variable 5) and a lower carotenoid concentration (variable 4), which could be related to the higher surface irradiance in this mesocosm. The difference in surface irradiance between the mesocosms, which could not be compensated by adjusting the height of the illumination boxes (Fig. 1), was caused by an unequal length of electrical wiring between the lamps and the 230 V to 12 V transformers. In future experiments, this is easily fixed and mesocosm reproducibility can be improved.

Additional mesocosm aspects

Constructing a mesocosm as presented in Fig. 1 is relatively simple. Apart from the metal frame and the illumination boxes that were built 'in-house' at the NIOZ, all mesocosms equipment used was 'of the shelf'. The cost of one complete mesocosm was 22 k€ (or 30 k$), of which the optical (irradiance and radiance) equipment took up 83%. Because of the heat from the lamps and the transformers, the construction should be placed in a room that is temperature-controlled and, in addition, the mesocosm frame should be open to allow rapid heat exchange. As a consequence, the water surface is exposed to contamination from dust particles, excluding tests of trace metal limitation or axenic (bacteria-free) experiments. On the other hand, the present configuration gives ample opportunity to manipulate the spatial orientation of the radiometers. Furthermore, a 0.5 × 0.5 m frame (not shown) that can hold filters to attenuate specific parts of the light spectrum can easily be placed below the illumination box (Fig. 1).

Models of absorption and fluorescence

Absorption and fluorescence in the mesocosms during the *Phaeocystis* experiment was examined by 1) an attenuation model including absorption and scattering and 2) modeling the fluorescence emission.

First, an attenuation model was constructed to describe the energy balance of a mesocosm filled with filtered seawater at

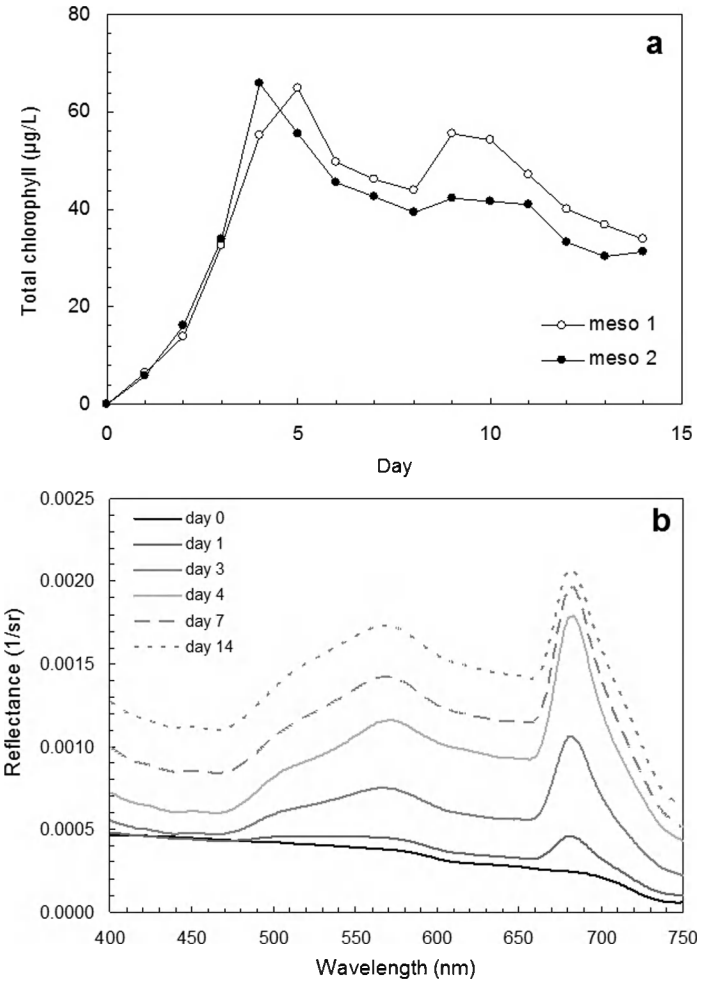

Fig. 5. Development of *Phaeocystis* biomass in a duplicate mesocosm experiment. a. Sum of the concentrations of chlorophylls *a*, c2, and c3. Mesocosm 1 received a nitrogen spike on day 8. b. Reflectance spectra calculated from water-leaving radiance from mesocosm 1. For clarity, only the data of 6 d is shown.

midday (maximum irradiance). The bottom irradiance (E_{bottom}) is approximated by a function of the surface irradiance (E_{top}) as:

$$E_{bottom} = E_{top} \times Loss \times \exp\left[-P_d x\, D \times (a_{tot} + b_{tot})\right] \quad (1)$$

Loss stands for the irradiance loss due to the air-water interface and geometry. P_d is the path-length of down-welling irradiation in the water, and D is water column height (0.70 m). With the exception of D, all variables are wavelength-dependent. The total absorption (a_{tot}, m^{-1}) is defined by the sum of absorption (m^{-1}) by pure water (W), the phytoplankton pigments (CHL), colored dissolved organic matter (CDOM), and detritus (DET):

$$a_{tot} = a_W + a_{CHL} + a_{CDOM} + a_{DET} \quad (2)$$

The total scattering (b_{tot}, m^{-1}) is determined by the scattering of pure water (W), the cell structure of the phytoplankton (CHL), and theoretically, remnants of cell structures in the detritus fraction (DET):

$$b_{tot} = b_W + b_{CHL} + b_{DET} \quad (3)$$

Temperature-corrected values of water absorption and scattering were taken from the literature (Buiteveld et al. 1994). The influence of the scattering coefficient of pure water was small. At maximum (400 nm), b_w equalled 0.0053 m^{-1}, which gave an additional scattering term of at 0.5% and, therefore, it played no role in the attenuation of the light in the mesocosm.

Figure 6 shows the measured surface and bottom irradiance as well as the modeled bottom irradiance of mesocosm 1 using Eq. 1. The spectral fit between 400 and 500 nm was slightly improved by assuming a weak absorption by CDOM of 0.04 m^{-1} at 440 nm and fixed slope of 0.016 (Twardowski et al. 2004). The strong attenuation by water above 700 nm could only be modeled if a P_d of 1.09 was assumed (a parallel beam of light has a P_d = 1.00), which corresponds to an angle (in water) of 23°. Loss consisted of a 2.6% loss by Fresnel reflection at the air-water interface and a 3.85% geometric loss. The average deviation between modeled and measured spectrum was 0.9 mW m^{-2} nm^{-1}(<1%) over the interval 400-720 nm. In this model, the absorption of pure water equals 0.43 m^{-1} at 682 nm, the central wavelength of fluorescence emission by the PSII system (Buiteveld et al. 1994).

Next, the potential fluorescence radiation was calculated. Because the conversion of energy in the cell takes place at the quantum level, the measured irradiance was converted from mW m^{-2} nm^{-1} to µmol photons m^{-2} s^{-1} nm^{-1}. One µmol of photons at 550 nm equals 0.217537 J, and the conversion is inversely proportional to the wavelength (Mobley 1994). The spectrum was integrated to yield the potential active radiation (PAR, 400-700 nm) and the potential fluorescence radiation (PFR, 400-672 nm). The stricter upper limit of 672 nm was based on a central fluorescence emission at 682 nm and a Stokes shift of 10 nm that determined the minimum extra energy needed for the excitation of a chlorophyll molecule. For the spectra shown in Fig. 6, the surface E_{top} had a PAR of 187 µmol photons m^{-2} s^{-1} and a PFR of 166 µmol photons m^{-2} s^{-1}. E_{bottom} without phytoplankton had a PAR of 151 µmol photons m^{-2} s^{-1} and a PFR of 138 µmol photons m^{-2} s^{-1}.

Daily PFR values are shown in Fig. 7. PFR-surface was the irradiance that was available to the mesocosm. The stability of the lamps was monitored continuously and proved to be constant (Fig. 2). PFR-water was the irradiance at the bottom of the mesocosm without phytoplankton, as measured and modeled for day zero (Fig. 6). PFR-bottom was the irradiance that was actually measured by the bottom sensor. Clearly, the phytoplankton provided additional attenuation in the mesocosms, approximately 100 µmol photons m^{-2} s^{-1} after day 4 (Fig. 7).

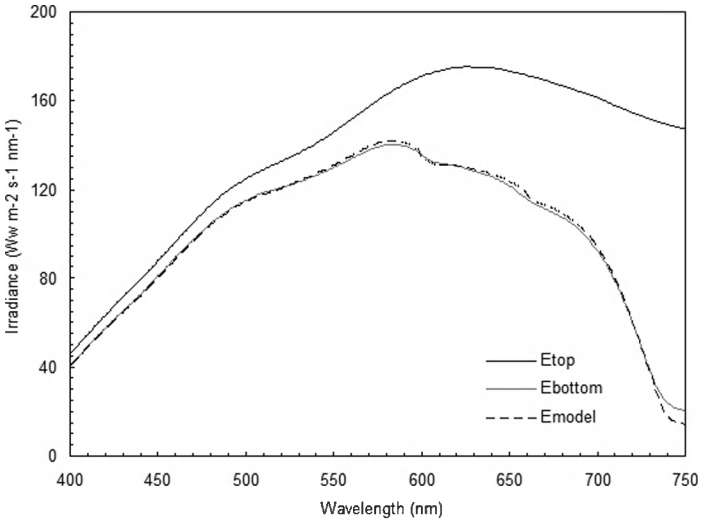

Fig. 6. The irradiance spectra at the top (Etop) and bottom (Ebottom) of mesocosm 1 filled with pure seawater on day zero of the *Phaeocystis* experiment. The dashed line (Emodel) is the attenuation model (Eq. 1) result. A comparable model result was achieved with mesocosm 2 data. 146 × 112 mm.

The attenuation of irradiance in the mesocosms (Eq. 1) is influenced by absorption (Eq. 2) and scattering (Eq. 3). In case there is no scattering (besides pure water), the radiation available for conversion to fluorescence at day (x) is equal to (PFR_0 – PFR_x), the PFR-irradiance at that day, corrected for the PFR-irradiance for pure water, measured at day (0). In case there is significant scattering in the mesocosms, this number is an upper limit for the PFR absorbed by the phytoplankton. The importance of scatter can be deduced from the reflectance spectra (Fig. 5b) that show a continuous increase of reflectance in the blue region of the spectrum, despite an increasing absorption due to higher chlorophyll concentrations. The magnitude of the scattering at all wavelengths was derived by introducing the independently measured ICAM a_{CHL} absorption spectra in Eq. 1. As an example, Fig. 8 shows the measurements and models for day four of the experiment. The difference between the measurement at day zero and day four shows that at all wavelengths irradiance was extremely reduced. Including a_{CHL} in the model predicted a too high irradiance or, in other words, the measurements were well below any model including the ICAM data. However, when the model included an additional white-scattering (i.e., wavelength independent) term, by increasing the 3.85% geometric loss to 43%, a satisfactory solution to the model could be obtained (Fig. 8).

The influence of scattering on the measured PFR was investigated in some more detail. PFR-bottom modeled with only ICAM absorption (a_{CHL}) showed that, from day 4 onward, about half the attenuation in the mesocosms was due to absorption and, therefore, half must be due to scattering (Fig. 7). The importance of scattering in PFR attenuation in the

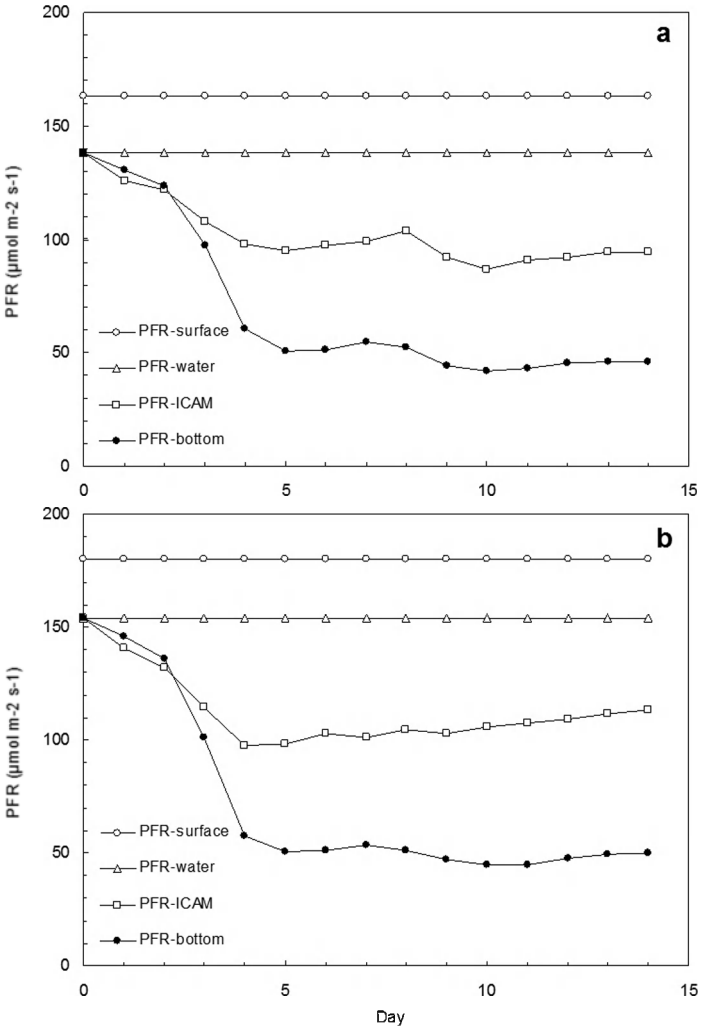

Fig. 7. Daily Potential Fluorescence Radiation (PFR, 400–672 nm) values for (a) mesocosm 1 and (b) mesocosm 2. PFR-surface is the irradiance that was available to the mesocosm. PFR-water is the irradiance at the bottom of the mesocosm on day zero. PFR-bottom is the irradiance that was actually measured by the bottom sensor. PFR-ICAM was modeled with only ICAM absorption (aCHL) included in the model, showing that ≈50% of PFR was absorbed by the phytoplankton.

Phaeocystis mesocosms was confirmed by the water-leaving radiance measurements. These were used to estimate the upward energy flux, the backscattered fraction of the total energy that was scattered in the mesocosm. In other words, the loss of scatter energy was the difference between the modeled PFR including the ICAM absorption and PFR_{bottom} in Fig. 7. Assuming a Q-factor of 3.14, the backscatter was well correlated to the total scattered radiation with a backscatter ratio of 0.015 (Fig. 9). This number was fully consistent with published values (0.005–0.021) for *Phaeocystis* (Lubac et al. 2008).

In the second step, the fluorescence emission was modeled. The fluorescence quantum efficiency (φ) of phytoplankton is defined as the ratio of mol photons emitted as fluorescence divided by the moles photons absorbed by the pigments (Huot

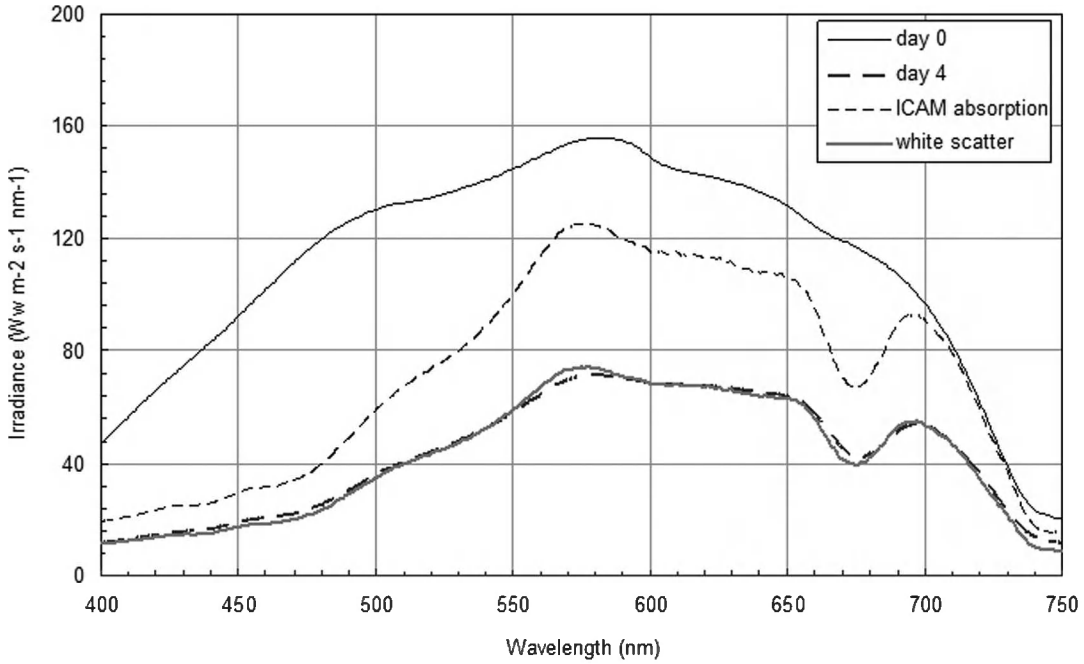

Fig. 8. Measured spectra of bottom PFR on day zero and four in mesocosm 2 compared with modeled data. Inclusion of aCHL as measured by the ICAM on day four in the model reduces PFR considerably. After including an additional white-scatter, the model satisfactorily reproduced the measured PFR on day four.

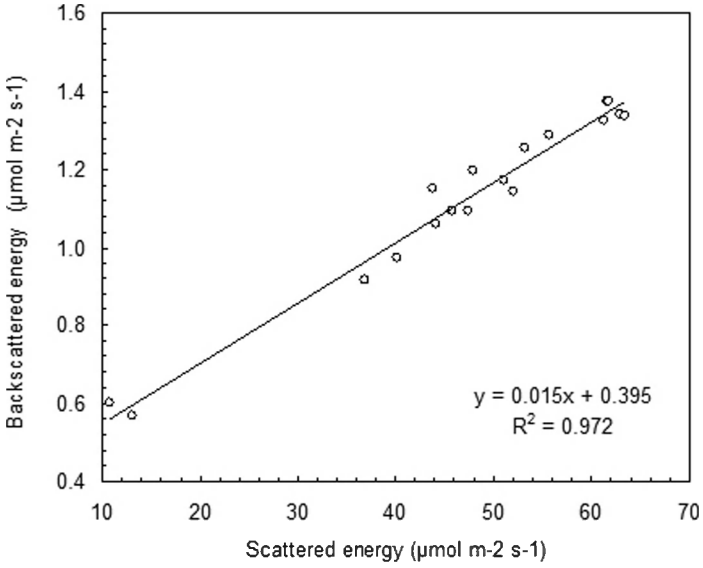

Fig. 9. Correlation between the PFR that is scattered in the mesocosm and the PFR that is scattered in the upward direction. The backscatter ratio is 0.015. Data from both Phaeocystis mesocosms.

et al. 2005). Measured values of φ are in the order of 1% (Behrenfeld et al. 2009; Huot et al. 2005) and, therefore, an emission in the order of 1 µmol photons m^{-2} s^{-1}, equal to 176 mW m^{-2} at 682 nm was expected. Because the emission is isotropic, this value has to be divided by 4π sr to yield a radiance of 14 mW m^{-2} sr^{-1}.

The pure fluorescence signal is emitted over a range of wavelengths, and the signal can be described by a Gaussian curve with a full width halve maximum of 25 nm (Mobley 1994). For this Gauss curve with a maximum height of 1 at 682 nm, the integral under the curve equals 26.6. This would imply that a fluorescence of 1 µmol photons m^{-2} s^{-1} could be detected as a Gaussian-shape emission with a maximum of 14/26.6 ≈ 0.5 mW m^{-2} sr^{-1} nm^{-1}. The modeled fluorescence emission, after it has been absorbed by water with a depth of 50, 100, and 200 cm, is given in Fig. 10a. From the modeled fluorescence curves in Fig. 10a, it can be seen that the contribution to the measured radiance was negligible outside the domain between 650 and 710 nm.

The fluorescence algorithms used by the MODIS and MERIS instruments retrieve the fluorescence signal (R_{fl}) by extracting a baseline reflectance R_{base} from the measured reflectance (R). When applied to the wavelength of maximum fluorescence (682 nm), the so-called fluorescence line height (FLH) can be derived (Abbott and Letelier 1999). The baseline was subtracted by taking a straight line between the reflection at 650 and 710 nm:

$$R_{fl} = R - R_{base}\ (sr^{-1}) \quad (4a)$$

with

$$R_{base} = R_{710} + (710 - \lambda) \times [(R_{650} - R_{710})/60] \quad (4b)$$

where λ is the wavelength

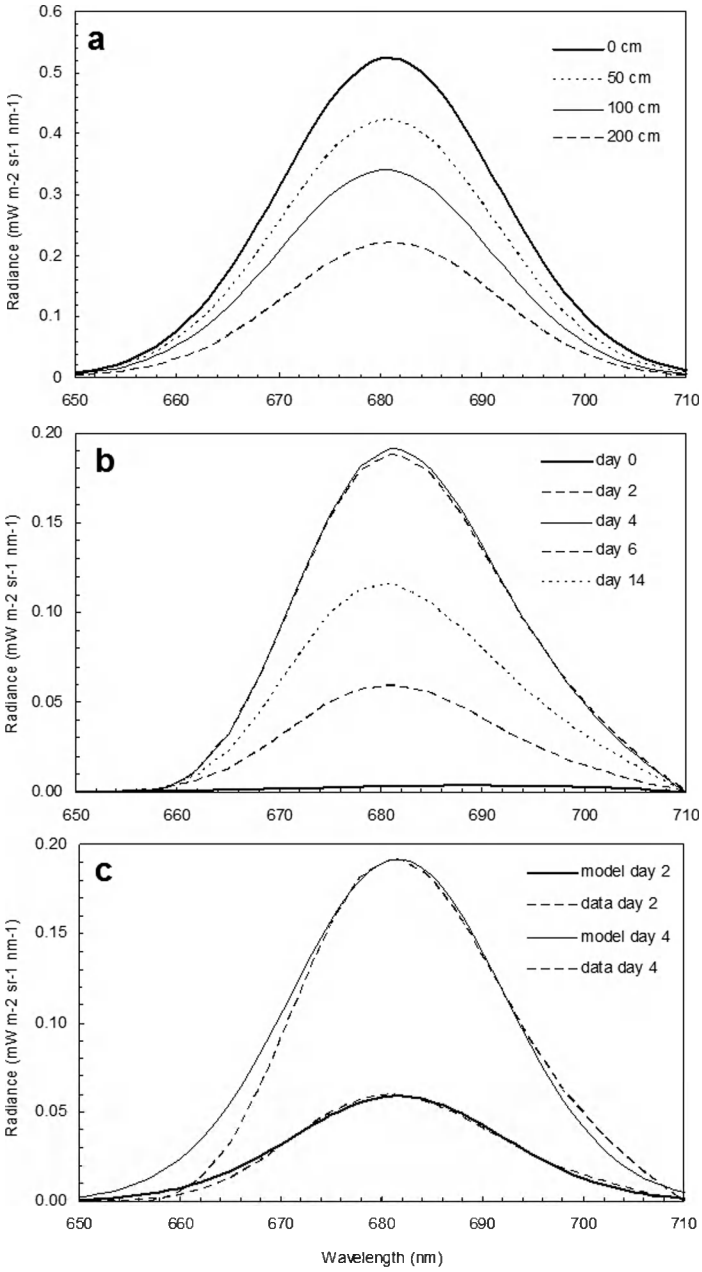

Fig. 10. Fluorescence radiance. a. Model spectra from an integrated flux of 1 µmol photons m^{-2} s^{-1}, eminating from different depths in the mesocosm. b. Measured spectra in the mesocosm (*Phaeocystis*). c. Comparison of modeled (50 cm depth) and measured radiance spectra for day two and day four in the mesocosm.

Subsequently, R_{fl} was multiplied with the surface irradiance to obtain the baseline corrected radiance. In Fig. 10b, examples of this corrected radiance were plotted for days 0 to 14 in mesocosm 2. Note that the signal at day zero was almost negligible. The signal clearly increased in the first days of the experiment (Fig. 10b).

In Fig. 10c, the Gaussian fluorescence model was compared with the baseline-corrected radiance. Because the radiance sensor was mounted above water, the radiance below water had to be multiplied by a factor 0.54 that corrected for the internal reflection at the water-air transition (2.6% loss) and the refraction at the water-air interface ($1/N^2$, with N the breaking index of water ≈ 1.34). In the simulation a mean water-column depth of 50 cm was assumed. Because of the linear baseline correction, while the water absorption increases nonlinearly with wavelength, minor deviations between model and measurement were detected above 682 nm. Below 682 nm, it was clear that re-absorption by phytoplankton became more prominent at higher cell concentrations. This was demonstrated by the overestimation of the model between 660 and 680 nm. When the re-absorption was included, the estimated emission increased between 8% and 29% with an average of 17%, fully in line with the estimates reported in literature (Babin et al. 1996).

Model validation

The modeled absorption and fluorescence radiation were compared with *Phaeocystis* biomass to examine if the calculations lead to values that are comparable to 'true' HPLC-determined biomass estimations. The exponential increase in chlorophyll concentration in the first 4 d of the experiment (Fig. 5a) lead to sharp increases in both absorbed and fluoresced radiation (Fig. 11). In addition, the decrease in chlorophyll concentrations after day 5 in both mesocosms, as well as the effect of the nitrogen spike to mesocosm 1 on day 8, resulting in a direct biomass increase on day 9, was shown in both absorption (Fig. 11a) and fluorescence (Fig. 11b). Therefore, the phytoplankton dynamics in the mesocosms were well described by absorption and fluorescence estimates.

The correlations between modeled absorption and fluorescence radiation and *Phaeocystis* biomass are shown in Fig. 12. The explained variance was high in both absorption (74%) and fluorescence (80%). On the other hand, linearity appeared to be lost at chlorophyll concentrations higher than 50 µg/L, resulting in a positive intercept in both Fig. 12a and 12b. In addition, and according to expectation due to the differences in nitrogen loadings, the two mesocosms behaved differently, especially in fluorescence. The fluorescence values in mesocosm 2, not spiked with nitrogen, were considerably higher than in N-spiked mesocosm 1 (Fig. 12b). This might be related to an increase in the quantum efficiency of fluorescence (φ) due to nutrient-stress (Falkowski et al. 1992). In addition, changes in the composition of fluorescent and non-fluorescent pigments in the phytoplankton must be taken into account (Peperzak et al. unpub. data). Values of φ ranged from 0.008 to 0.016 (Peperzak et al. unpub. data) and are comparable to real-world estimates derived from satellite observations (Behrenfeld et al. 2009; Huot et al. 2005; Peperzak et al. unpub. data). Fig. 12 shows that absorption and fluorescence measurements were adequately sensitive to determine phytoplankton biomass at low (≈1 µg/L) chlorophyll concentrations.

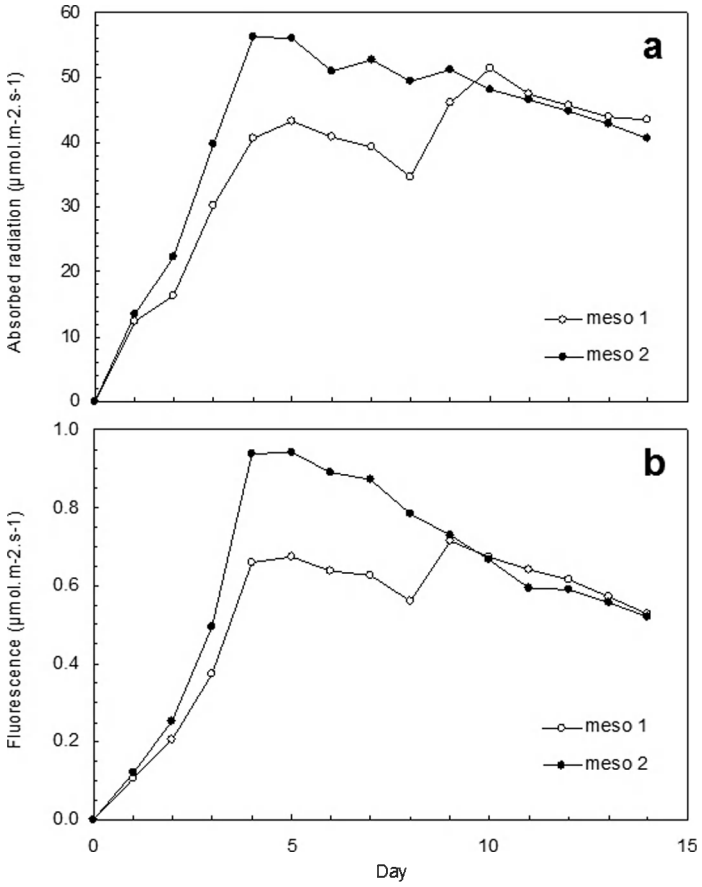

Fig. 11. Absorbed radiation (a) and emmitted fluorescence (b) during the *Phaeocystis* experiment. Absorbed radiation was calculated from surface irradiance and ICAM absorption. Fluorescence was calculated from water-leaving radiance.

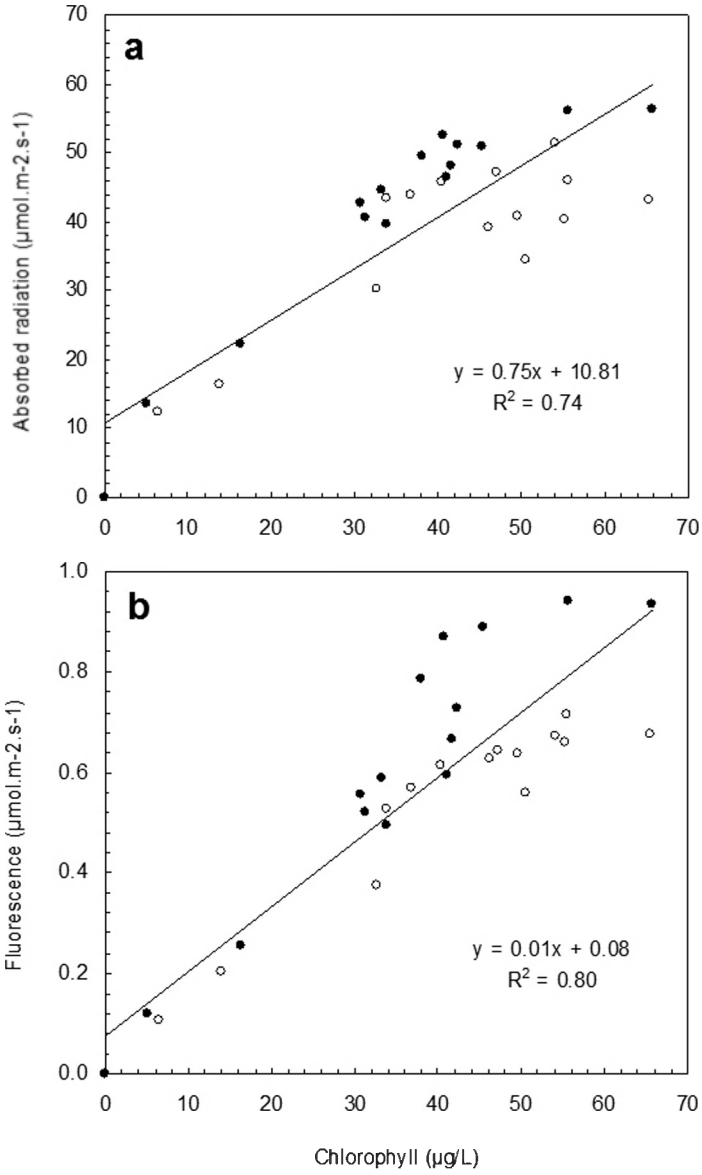

Fig. 12. Correlations between *Phaeocystis* in situ (biomass) and optical (a) absorption and (b) fluorescence measurements. Biomass is the sum of HPLC-measured chlorophyll *a*, -c1 and -c3 concentrations. Absorbed radiation was calculated from surface irradiance and ICAM absorption. Fluorescence was calculated from water-leaving radiance. The linear regression line in both a and b was calculated using the data of both mesocosm 1 (○) and mesocosm 2 (●).

Discussion

The basic aim of the experimental set-up was, under controlled but semi-natural conditions, to allow manipulated phytoplankton growth in a vessel large enough to perform both remote-sensing observations and in situ (water-) sampling. In the mesocosms, it has been possible under temperate conditions of irradiance, temperature, and turbulence to grow biogeochemically-relevant species as *E. huxleyi* and *P. globosa*. Duplicate mesocosm showed good precision (±20%) with room for improvement by fine-tuning of the illumination. A test with duplicate sensors also showed good precision (<5% deviation). The accuracy of chlorophyll estimates by absorption and fluorescence was 74% to 80%, respectively (variance explained), although it was negatively influenced by changes in the physiological condition of the phytoplankton, notably in the pigment composition (Peperzak et al. unpub. data). The biomass detection limit was ≈1 µg chlorophyll/L, which is sufficient for simulations of nonoligotrophic waters. An apparent loss of linearity above 50 µg chlorophyll/L was detected, but effects of changes in the quantum efficiency of fluorescence and of changes in the composition of fluorescent and non-fluorescent pigments were not yet taken into account. Accuracy and linearity may, therefore, be further improved. Estimates of the quantum efficiency of fluorescence (φ) were comparable to real-world estimates derived from satellite observations. In conclusion, the mesocosms described here (Fig. 1) allow for the accurate and precise measurement, by optical instruments, of controlled phytoplankton dynamics under semi-natural conditions.

Within the temperature limits of the climate room, the mesocosms were placed (10 to 25°C), a wide range of irradiances (0 to 45 W m^{-2}) and light:dark cycles (0:24 to 24:0 hour d^{-1}) can be applied. Therefore, the mesocosms show great potential for the experimental manipulation of a large range of temperate to tropical phytoplankton with the simultaneous observation with optical instruments. So far, the growth of only two phytoplankton species, *E. huxleyi* and *P. globosa*, that belong to different plankton functional types (PFTs) were investigated. In recent years, it has been shown that it is possible to distinguish PFTs by satellite remote sensing (Nair et al. 2008; Sathyendranath et al. 2004). The mesocosm introduced in the present study has the capability to experiment with PFTs, either as single cultures or as species mixtures, and to examine their optical properties. In addition, the mesocosm should be able to generate experimental data on the functional responses of both autotrophic and heterotrophic PFTs, such as growth and grazing rates as a function of irradiance, nutrients, pH, and food concentrations. These rate parameters, which are presently poorly constrained in dynamic green ocean models (DGOMs) (Le Quere et al. 2009), can be examined simultaneously in the mesocosm by both in situ and optical methodologies. In addition, there are no restrictions to use and manipulate experimental mixtures or complex natural water samples that may include viruses, phytoplankton, and zooplankton. It is anticipated that the mesocosms presented here have great potential in combining experimental data on phytoplankton composition, dynamics, and associated biogeochemical cycling with remotely sensed proxies, thereby bridging the gap between in vitro experiments and real-world satellite measurements.

Comments and recommendations

A next step in processing water-leaving radiance from the mesocosms is to develop algorithms for phytoplankton absorption, rather than using an ICAM, in order to be able to compare both absorption and fluorescence with satellite imagery.

References

Abbott, M. R., and R. M. Letelier. 1999. Algorithm theoretical basis document chlorophyll fluorescence (MODIS product number 20). NASA.

Abraham, E. R., C. S. Law, P. W. Boyd, S. J. Lavender, M. T. Maldonado, and A. R. Bowle. 2000. Importance of stirring in the development of an iron-fertilized phytoplankton bloom. Nature 407:727-730 [doi:10.1038/35037555].

Babin, M., A. Morel, and B. Gentili. 1996. Remote sensing of sea surface sun-induced chlorophyll fluorescence: consequences of natural variations in the optical characteristics of phytoplankton and the quantum yield of chlorophyll a fluorescence. Int. J. Rem. Sens. 17:2417-2448 [doi:10.1080/01431169608948781].

Behrenfeld, M. J., and others. 2009. Satellite-detected fluorescence reveals global physiology of ocean phytoplankton. Biogeosciences 6:779-794 [doi:10.5194/bg-6-779-2009].

Belzile, C., and others. 1998. An experimental tool to study the effects of ultraviolet radiation on planktonic communities: a mesocosm approach. Environ. Technol. 19:667-682 [doi:10.1080/09593331908616723].

Buiteveld, H., J. M. H. Hakvoort, and M. Donze. 1994. The optical properties of pure water, p. 174-183. *In* J. S. Jaffe [ed.], Ocean optics XII. SPIE, Vol. 2258.

Carder, K. L., R. Chen, and S. Hawes. 2003. Algorithm theoretical basis document: Instantaneous photosynthetically available radiation and absorbed radiation by phytoplankton. Version 7. NASA.

Claustre, H., and others. 2002. Diel variations in Prochlorococcus optical properties. Limnol. Oceanogr. 47:1637-1647 [doi:10.4319/lo.2002.47.6.1637].

Costello, D. K., K. L. Carder, and W. Hou. 1995. Aggregation of diatom bloom in a mesocosm: Bulk and individual particle optical measurements. Deep Sea Res. II 42:29-45 [doi:10.1016/0967-0645(95)00003-9].

Cui, T., J. Zhang, H. Zhang, Y. Ma, and X. Gao. 2003. Spectral characteristics analysis of red tide water in mesocosm experiment, p. 287-294. *In* R. J. Frouin, Y. Yuan, H. Kawamura [eds.], Ocean remote sensing and applications. Proceedings of SPIE, Vol 4892.

Escaravage, V., L. Peperzak, T. C. Prins, J. C. H. Peeters, and J. C. A. Joordens. 1995. The development of a *Phaeocystis* sp. bloom in a mesocosm experiment in relation to nutrients, irradiance and coexisting algae. Ophelia 42:55-74.

Esposito, S. 2006. Numerical studies on phytoplankton responses in the ocean mixed layer. Universita degli studi di Napoli "Frederico II."

Falkowski, P., R. M. Greene, and R. Geider. 1992. Physiological limitations on phytoplankton productivity in the ocean. Oceanogr. Mar. Biol. 5:84-91.

Gieskes, W. W. C., and G. W. Kraay. 1986. Analysis of phytoplankton pigments by HPLC before, during and after mass occurrence of the microflagellate Corymbellus aureus during the spring bloom in the open northern North Sea in 1983. Mar. Biol. 92:45-52 [doi:10.1007/BF00392744].

Grashoff, K., M. Ehrhardt, and K. Kremling. 1983. Methods of seawater analysis. Chemie GmbH.

Helder, W., and R. De Vries. 1979. An automatic phenol-hypochlorite method for the determination of ammonia in sea- and brackish waters. Neth. J. Sea Res. 13:154-160 [doi:10.1016/0077-7579(79)90038-3].

Hunter, P. D., A. N. Tyler, M. Présing, A. W. Kovács, and T. Preston. 2008. Spectral dicrimination of phytoplankton colour groups: The effect of suspended particulate matter and sensor spectral resolution. Rem. Sens. Environ. 112:1527-1544 [doi:10.1016/j.rse.2007.08.003].

Huot, Y., C. A. Brown, and J. J. Cullen. 2005. New algorithms for MODIS sun-induced chlorophyll fluorescence and a comparison with present data products. Limnol. Oceanogr.:

Methods 3:108-130 [doi:10.4319/lom.2005.3.108].

Kirk, J. T. O. 1994. Light and photosynthesis in aquatic ecosystems. Cambridge Univ. Press [doi:10.1017/CBO9780511623370].

Le Quéré, C., and others. 2009. Observational needs of dynamic green ocean models. <https://abstracts.congrex.com/scripts/jmevent/abstracts/FCXNL-09A02a-1718716-2-Le_Quere_et_al_OceanObs09_final_formatted.pdf>.

Lubac, B., H. Loisel, N. Guiselin, R. Astoreca, L. F. Artigas, and X. Meriaux. 2008. Hyperspectral and multispectral ocean color inversions to detect *Phaeocystis globosa* blooms in coastal waters. J. Geophys. Res. 113: C06026 [doi:10.1029/2007JC004451].

Mobley, C. D. 1994. Light and water, radiative transfer in natural waters. Academic Press.

Murphy, J., and J. P. Riley. 1962. A modified single solution method for the determination of phosphate in natural waters. Anal. Chim. Acta 27:31-36 [doi:10.1016/S0003-2670(00)88444-5].

Nair, A., and others. 2008. Remote sensing of phytoplankton functional types. Rem. Sens. Environ. 112:3366-3375 [doi:10.1016/j.rse.2008.01.021].

O'Reilly, J. E., and others. 1998. Ocean color chlorophyll algorithms for SeaWIFS. J. Geophys. Res. 103:24937-24953.

Parkinson, C. L., and R. Greenstone. 2000. EOS data products handbook. NASA/Goddard Space Flight Center.

Peperzak, L. 1993. Daily irradiance governs growth rate and colony formation of *Phaeocystis* (Prymnesiophyceae). J. Plankton Res. 15:809-821 [doi:10.1093/plankt/15.7.809].

Peperzak, L., R. N. M. Duin, F. Colijn, and W. W. C. Gieskes. 2000a. Growth and mortality of flagellates and non-flagellated cells of *Phaeocystis globosa* (Prymnesiophyceae). J. Plankton Res. 22:107-119 [doi:10.1093/plankt/22.1.107].

———, E. G. Vrieling, B. Sandee, and T. Rutten. 2000b. Immuno flow cytometry in marine phytoplankton research. Scient. Marina 64:165-181.

Röttgers, R., C. Häse, and R. Doerffer. 2007. Determination of the particulate absorption of microalgae using a point-source integrating-cavity absorption meter: verification with a photometric technique, improvements for pigment bleaching and correction for chlorophyll fluorescence Limnol. Oceanogr. Methods 5:1-12 [doi:10.4319/lom.2007.5.1].

Sathyendranath, S., L. Watts, E. Devred, T. Platt, C. Caverhill, and H. Maass. 2004. Discrimination of diatoms from other phytoplankton using ocean-colour data. Mar. Ecol. Prog. Ser. 272:59-68 [doi:10.3354/meps272059].

Schalles, J. F., D. C. Rundquist, and F. R. Sciebe. 2001. The influence of suspended clays on phytoplankton reflectance signatures and the remote estimation of chlorophyll. Verh. Internat. Verein Limnol. 27:3619-3625.

Schreiber, U., U. Schliwa, and W. Bilger. 1986. Continuous recording of photochemical and non-photochemical chlorophyll fluorescence quenching with a new type of modulation fluorometer. Photosynth. Res. 10:51-62 [doi:10.1007/BF00024185].

Strickland, J. D. H., and T. R. Parsons. 1968. A practical handbook of seawater analysis, first ed. Fisheries Research Board of Canada.

Twardowski, M. S., E. Boss, J. M. Sullivan, and P. L. Donaghay. 2004. Modeling the spectral shape of absorption by chromophoric dissolved organic matter. Mar. Chem. 89:69-88 [doi:10.1016/j.marchem.2004.02.008].

Van Der Woerd, H. J., and R. Pasterkamp. 2008. HYDROPT: A fast and flexible method to retrieve Chl a from multispectral satellite observations of optically complex coastal waters. Remote Sens. Environ. 112:1795-1807 [doi:10.1016/j.rse.2007.09.001].

Vaulot, D., and D. Marie. 1999. Diel variability of photosynthetic picoplankton in the equatorial Pacific. J. Geophys. Res. 104:3297-3310 [doi:10.1029/98JC01333].

Zapata, M., F. Rodríguez, and J. L. Garrido. 2000. Separation of chlorophylls and caretenoids from marine phytoplankton: a new HPLC method using a reversed phase C8 column and pyridine-containing mobile phases. Mar. Ecol. Prog. Ser. 195:29-45 [doi:10.3354/meps195029].

———, S. W. Jeffrey, S. W. Wright, F. Rodríguez, J. L. Garrido, and L. Clementson. 2004. Photosynthetic pigments in 37 species (65 strains) of Haptophyta: implications for oceanography and chemotaxonomy. Mar. Ecol. Prog. Ser. 270:83-102 [doi:10.3354/meps270083].

Submitted 11 June 2010
Revised 19 April 2011
Accepted5 May 2011